sustainability

MDPI

Article

Nonlinear Enhanced Control for Wind Energy Generation System-Based Permanent Magnet Synchronous Generator

Youssef Errami [1,*], Abdellatif Obbadi [1], Smail Sahnoun [1] and Mohssin Aoutoul [2]

[1] Laboratory of Electronics, Instrumentation and Energy, Faculty of Science, University Chouaib Doukkali-Eljadida, El Jadida 24000, Morocco; obbadi.a@ucd.ac.ma (A.O.); sahnoun.s@ucd.ac.ma (S.S.)
[2] Laboratory of STIC, Faculty of Science, University Chouaib Doukkali-Eljadida, El Jadida 24000, Morocco; mohssin.aoutoul@gmail.com
* Correspondence: errami.y@ucd.ac.ma

Abstract: This paper proposes a Nonlinear Backstepping Approach (NBA) to improve the control performance of a Permanent Magnet Synchronous Generator (PMSG)-based Wind Energy Generation System (WEGS) under parameter uncertainties and short circuits with fluctuations in the grid voltage. Both the rectifier and the three-phase inverter are controlled using the NBA scheme; this method ensures Maximum Power Point Tracking (MPPT), which is a very appealing control objective with unpredictable scenarios of wind speed, and regulates the active and reactive power flows to the electrical network under varying wind speeds. Also, an inverter was employed to control voltage of the DC bus and the powers. The regulator's stability is achieving using the Lyapunov approach. Simulation results with Matlab/Simulink confirm the efficiency of the presented scheme. The comparative analysis of the NBA with conventional Vector Controllers (VCs), under parameter deviations and for low voltage drop conditions, demonstrates the efficiency of the studied method.

Keywords: PMSG; MPPT; backstepping theory; electrical grid

check for updates

Citation: Errami, Y.; Obbadi, A.; Sahnoun, S.; Aoutoul, M. Nonlinear Enhanced Control for Wind Energy Generation System-Based Permanent Magnet Synchronous Generator. *Sustainability* **2024**, *16*, 7374. https://doi.org/10.3390/su16177374

Academic Editor: Bowen Zhou

Received: 26 July 2024
Revised: 20 August 2024
Accepted: 22 August 2024
Published: 27 August 2024

Copyright: © 2024 by the authors. Licensee MDPI, Basel, Switzerland. This article is an open access article distributed under the terms and conditions of the Creative Commons Attribution (CC BY) license (https://creativecommons.org/licenses/by/4.0/).

1. Introduction

Recently, there has been a significant penetration of WEGSs into the power grid as they provide several benefits, including their low operational costs and a lower impact compared to other green energy infrastructures [1,2]. As such, they are performing essential tasks in the sustainable generation of power and will be developed more in the future. Also, at present, variable-speed WEGSs are the most common wind power generators and have been extensively used in wind power infrastructure. On the other hand, different types of generators are employed in WEGSs: the Induction Generator (IG), the Doubly Fed Induction Generator (DFIG) and the PMSG [3]. Further, the PMSG is generally preferred for wind generation applications. Its merits include the exclusion of DC excitation, the lack of a need for a gear box, high reliability, efficient construction, and its ability to simply ensure MPPT [4]. Also, the PMSG is the most appropriate generator for use at a low speeds because of the great number of rotor–pole pairs [5]. Creating an electrical network of PMSGs is possible by utilizing a full-scale Back-to-Back Converter (BTBC) [6]. Figure 1 shows the general control structure for a WEGS-based PMSG. The decoupling capacitor is utilized to disconnect the controls of both converters. The rectifier permits the speed, the torque and the power of the generator to be controlled. The inverter is employed for synchronization of the WEGS with the electrical network and for keeping constant the DC bus voltage. Also, it ensures the Unity Power Factor (UPF) of this WEGS. On the other hand, to guarantee the full benefit of the WEGS, a successful MPPT approach should be utilized. But, because of its intermittent and uncertain nature, a considerable penetration rate of wind energy can ruin the energy quality. So, in recent years and to resolve the abovementioned issues, several control theories have been studied. The classic Vector Control Approach (VCA) using Linear Controllers (LCs) such as Proportional Integral (PI) controllers is one of

the most important control methods, and it is still used in numerous WEGSs thanks to characteristics such as ease and stability. Hamid et al. [7], Shuhui et al. [8] and Duc-Tung et al. [9] have proposed extracting maximum power for wind system-based PMSGs. This approach ensures that the WEGS operates at its maximum power coefficient to ensure MPPT under varying wind states. In spite of the VC's excellent performance, it suffers from uncertainty, nonlinearity and variations in the parameter of the infrastructure. To surmount these disadvantages, Direct Power/Torque Control are utilized to replace the VCA for both rectifier and inverter control. This technique employs hysteresis regulators and uses the ideal switching combination of converters for enhanced dynamic response at varying wind speeds and load torques. In addition, look-up tables and comparators with hysteresis are utilized. Furthermore, it uses the minimization of the error between the references and actual values of powers. Rajaei et al. [10] have presented a DTC of the PMSG system using the Vienna rectifier and studied the influences of this technique on flux and torque of generator. Yurong et al. [11] and Zhenbin et al. [12] have proposed maximizing energy extraction using a DTC. Zhang et al. [13,14] have presented a DTC approach for PMSG wind energy infrastructure. Freire et al. [15] have presented a fault-tolerant generator drive. It utilizes direct control techniques to control WEGS-based PMSGs and to guarantee fault-tolerant aptitude. Therefore, the direct control approach is distinguished by a rapid dynamic response, the absence of the transformation of coordinates, a constantly switching frequency and a low influence on parameters. But, this technique creates large steady power ripples owing to the use of hysteresis comparators and look-up tables. Moreover, its performance degrades with low operating speeds. On the other hand, the power captured by this WEGS very much depends on the control strategies used, and a high proportion of wind energy will bring novel challenges to the control of power system. Also, the nonlinear properties of the synchronous generator, uncertainties of parameters and exterior disturbances make the controller procedure very complex. To address this problem, diverse control strategies have been proposed. So, Bakhtiari et al. [16] proposed the Feedback Optimal Controller (FOC) and the Extended Kalman Filter (EKF) to support the MPPT technique with frequent disturbances for wind system-based PMSGs. Belkhier et al. [17] presented MPPT, for wind energy-based PMSG, with the Adaptive Passivity-based Modifed Super Twisting approach (APMST) with fuzzy logic theory. As a result, MPPT, integration into the electrical grid and control of the power are ensured. Much research has been developed using nonlinear control techniques for wind energy systems that are not sensitive to changes in the system's parameters and exterior perturbations. Several nonlinear control schemes are utilized. Osman et al. [4] proposed Sliding Mode Control (SMC) for WEGS-based PMSGs with LCL and RL filters. The chosen techniques reduce the chattering effect and minimize the grid currents' harmonic distortion. Reactive power control is also employed to inject a reactive current into the electrical network, to serve voltage recuperation and to sustain the stability of grid. Pan et al. [18] presented SMC using an Extended State Observer (ESO) applied to control an offshore wind farm. This technique is employed to improve MPPT via aerodynamic torque estimation. Authors in [19] used a torque control strategy and first integral SMC to develop an MPPT technique. Meanwhile, the Nonlinear Backstepping Approach (NBA) is applied in many power structures owing to its excellent dynamic response, robustness and effective control characteristics under different operating conditions. The design of this method is based on feedback in order to ensure the control. Indeed, the goal is to stabilize a state of virtual control by decomposing the nonlinear control structure, which is complex, into recursive subsystems that are simpler and smaller. Thus, the control rules are implemented gradually. Also, this approach ensures a better transient response and a reduction in the complexity of the controller, and it is robust against system uncertainties and parametric fluctuations. Wang et al. [20] have proposed NBA for the converter with High Voltage Direct Current (HVDC). As a result, a stable HVDC bus for the grid and Unity Power Factor (UPF) were ensured. In [21], MPPT with NBA is reported to ensure MPPT for WEGSs. This work proposes using the NBA for control performance improvement of a PMSG-based WEGS under the conditions of

voltage fluctuations and short circuits in the electrical network and parameter uncertainties. Figure 1 shows the developed structure. The Generator Side Converter (GSC) is in charge of controlling the PMSG's speed. The optimal velocity tracking of the synchronous generator for MPPT is realized by the NBA. Also, to evade excessive PMSG acceleration with elevated speed wind states, pitch angle system is functional to limit the captured wind energy and maintain the velocity at the value's reference. The inverter is expansively controlled by the NBA to combine both the regulation of the DC voltage and the adjustment of powers exchanged with the electrical grid to attain the UPF. The voltage of the DC bus ensures the power balance between the power injected into the PMSG side converter and the power transmitted to the inverter. The control approach requires two inner current loops, which are employed to control the current of the grid and to perform power factor correction. Also, an external voltage loop is utilized for keeping the DC bus voltage constant. The controller's stability is guaranteed by Lyapunov analysis. The proposed nonlinear approaches are compared in terms of robustness with respect the unknown uncertainties and grid fault with a conventional VC method-based PI controller. On the other hand, various nonlinear control methods have been employed in the literature, including Input Output Feedback Linearization (IOFL) [22] and Sliding Mode Control [23,24]. In [23], the first-order SMC technique was used to control a WEGS-based PMSG. However, an unfortunately high chattering phenomenon, which is caused by discontinuous function in SMC and which has negative effects on mechanical parts of a WEGS, occurs. Furthermore, during grid faults, in attenuation of DC link voltage takes place. In contrast to [24–26], while SMC has been considered to control only a single converter in the BTBC, in this study, the NBA was used to control both the GSC and MSC of the BTBC. This was able to better reduce the response time and improve robustness of the WEGS against variations in the system's parameters and exterior disturbances.

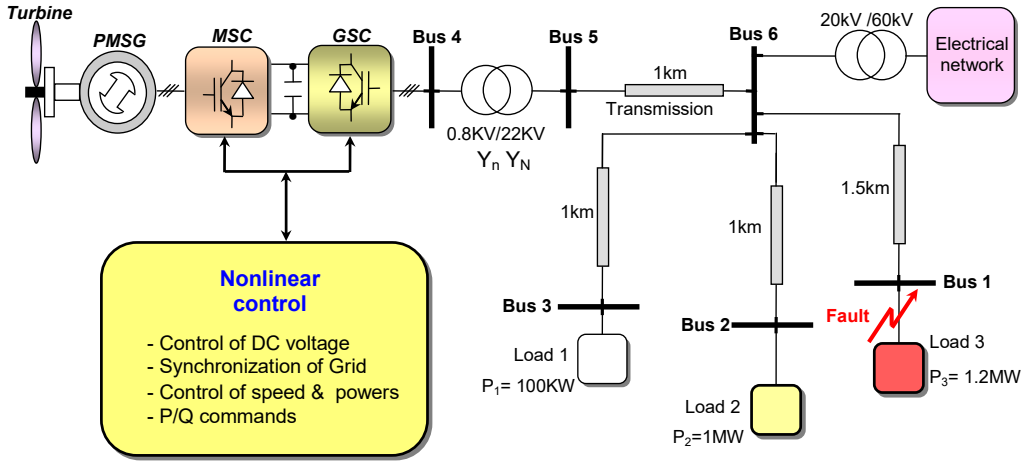

Figure 1. Nonlinear control for WEGS-based PMSGs.

The contributions of the paper can be summarized as follows:

1. The NBA is utilized for wind system-based PMSGs to ensure MPPT, to regulate DC-link voltage, to control powers exchanged with the grid and to ensure the UPF under diverse functioning conditions;
2. Improvement in response time, reference tracking precision and reduction in over-shoot;
3. Attainment of a high level of robustness against variations of parameters;
4. The WEGS's supervision can deal with low voltage drop conditions and model uncertainties;
5. The pitch angle system proposed can track the reference value of the speed and limit the captured wind energy if wind speeds are high;
6. Using the Lyapunov stability theory, some adequate conditions have been derived that guarantee the global asymptotical stability of the system.

Following the introduction, the model and control schemes developed for this WEGS are presented in Sections 2 and 3. The NBA scheme's performance is evaluated under diverse functioning conditions in Section 4, and the effectiveness of the NBA controller is compared with a conventional VC.

2. Modelling of WEGS

2.1. Wind Turbine (WT)

The actual mechanical power at the generator rotor is [21]:

$$P_{Turbine} = \frac{1}{2}\rho\pi R_t^2 C_p(\lambda,\beta)v_w^3 \tag{1}$$

where ρ is the density of the air, R_t is the radius of the WT blade and v_w is the speed of the wind. C_p characterizes the efficiency of the WT, which is called the coefficient of power. β is the Pitch Angle (PA) of the blade, and λ is the ratio between the speed of the blade and v_w, which is given as follows:

$$\lambda = \frac{\Omega_t R_t}{v_w} \tag{2}$$

where Ω_t is the speed of the blades. C_p can be represented by (3) [21]:

$$\begin{array}{l} C_p(\lambda,\beta) = \frac{1}{2}\left(\frac{116}{\lambda_c} - 0.4\beta - 5\right)e^{-\left(\frac{21}{\lambda_c}\right)} \\ \frac{1}{\lambda_c} = \frac{1}{\lambda+0.08\beta} - \frac{0.035}{\beta^3+1} \end{array} \tag{3}$$

Figure 2 shows the output power of the WT. So, whatever the wind speed, the WT must be rotated at an optimal speed which conducts to the optimal $\lambda = \lambda_{opti}$ and the optimal $C_p = C_{p-\max}$ to ensure maximum power extraction during various wind conditions. As a result, the MPPT mode is ensured [27]. In Figure 2, the curve in the MPPT state is represented. In addition, using Equation (2), the reference of speed can be defined by:

$$\Omega_{t-ref} = \frac{\lambda_{opti}.v_w}{R_t} \tag{4}$$

Finally, the maximum power can be extracted with:

$$P_{WT-\max} = \frac{1}{2}\rho\pi R_t^2 C_{p-\max}\left(\frac{R_t\Omega_{t-ref}}{\lambda_{opti}}\right)^3 \tag{5}$$

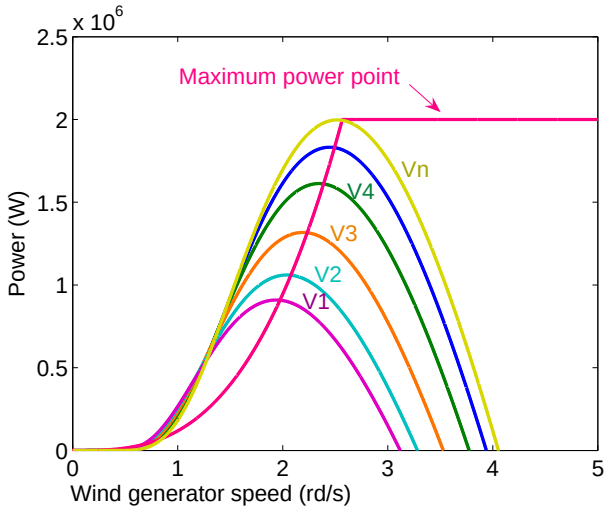

Figure 2. WT power curves.

2.2. Model of Generator and B2B Two-Level Converters

The model of the generator can be presented as [28]:

- Mechanical model:

$$J\frac{d\Omega_t}{dt} = \frac{3}{2}p_n\left[\psi_f i_q\right] - T_m - F\Omega_t \tag{6}$$

- Electrical model:

$$\frac{di_q}{dt} = \frac{1}{L_s}(v_{gq} - R_g i_q - \omega_e L_s i_d - \omega_e \psi_f) \tag{7}$$

$$\frac{di_d}{dt} = \frac{1}{L_s}(v_{gd} - R_g i_d + \omega_e L_s i_q) \tag{8}$$

$$\omega_e = p_n \Omega_t \tag{9}$$

where ω_e is the electrical rotating velocity of the PMSG, p_n is the number of the pole pair, v_{gq}, v_{gd} are the stator voltages, i_q, i_d are the d-q axis stator currents, L_s is the stator reactance of PMSG, R_g is the stator's resistance; ψ_f is the peak flux of the PMSG, J is total moment of inertia of the system, F is the coefficient of viscous friction and T_m is the turbine's torque.

2.3. Model of GSC

The grid dynamic model is [29]:

$$L_f\frac{di_{d-grid}}{dt} = e_d - V - R_f i_{d-grid} + \omega L_f i_{q-grid} \tag{10}$$

$$L_f\frac{di_{q-grid}}{dt} = e_q - \omega L_f i_{d-grid} - R_f i_{q-grid} \tag{11}$$

where e_d, e_q are GSC voltage components, i_{d-grid}, i_{q-grid} are the d-axis current and q-axis current of the grid, V is the grid voltage components in the d-axis and ω is the electrical frequency which is obtained using PLL. On the other hand:

$$C\frac{dU_{dc}}{dt} = i_0 - i_{dc} \tag{12}$$

where U_{dc} is the voltage of the DC link, i_{dc} is the current at the input of the inverter, i_0 is the output current of the PMSG and C is the capacitor of the DC link. The powers are [30]:

$$P_{grid} = \frac{3}{2}Vi_{d-f} \tag{13}$$

$$Q_{grid} = \frac{3}{2}Vi_{q-f} \tag{14}$$

3. Proposed Control of the WEGS

3.1. Control of MSC

For each wind speed, to ensure the maximum extraction of power from wind, λ must attain its optimum value λ_{opti}. So, the WT must be rotated at an optimal speed, Ω_{t-ref}, which is obtained from (4). On the other hand, according to (6), the speed of the PMSG can be controlled through i_q. So, the structure of the MSC control is reposed by an inner current control and an external speed control loop. This external loop controls the PMSG speed to guarantee the MPPT. The loops of the currents control the referenced d-q axis currents to their references. The control scheme is based on the NBA, which employs the implicit variable of control to create the primary simple system with high order. Also,

corresponding error variable is generated and can be stabilized by choosing the correct inputs for control. So, the error is:

$$\varepsilon_{\Omega} = \Omega_{t-ref} - \Omega_t \tag{15}$$

By taking one get the following expression:

$$\frac{d\varepsilon_{\Omega}}{dt} = \frac{d\Omega_{t-ref}}{dt} - \frac{d\Omega_t}{dt} \tag{16}$$

Based on (6), the time derivative of ε_{Ω}, is calculated as:

$$\frac{d\varepsilon_{\Omega}}{dt} = \frac{d\Omega_{t-ref}}{dt} - \frac{1}{J}\left(\frac{3}{2}p_n\left[\psi_f i_q\right] - T_m - F\Omega_t\right) \tag{17}$$

Additionally, the d-q axis current components are considered as the variables of virtual control. i_{d-r} is fixed at zero to reduce the copper failure and the WT velocity converges towards its reference Ω_{t-ref} if:

$$i_{d-r} = 0 \tag{18}$$

$$i_{q-r} = \frac{2}{3p_n\psi_f}(Jk_{\Omega}\varepsilon_{\Omega} + J\frac{d\Omega_{t-ref}}{dt} + F_v\Omega_t + T_m) \tag{19}$$

Then, we choose these errors:

$$\varepsilon_d = i_{d-r} - i_d \tag{20}$$

$$\varepsilon_q = i_{q-r} - i_q \tag{21}$$

Based on (7) and (8), the time derivatives of ε_d and ε_q are calculated as:

$$\frac{d\varepsilon_d}{dt} = \frac{di_{d-r}}{dt} - \frac{di_d}{dt} = -\frac{1}{L_s}(L_s\omega_e i_q + v_{gd} - R_g i_d) \tag{22}$$

$$\frac{d\varepsilon_q}{dt} = \frac{di_{q-r}}{dt} - \frac{di_q}{dt} = \frac{di_{q-r}}{dt} - \frac{1}{L_s}(v_{gq} - \omega_e\psi_f - R_g i_q - L_s\omega_e i_d) \tag{23}$$

To establish the stabilizing function, we choose the following Lyapunov function:

$$Y_{MSC} = \frac{1}{2}\varepsilon_{\Omega}^2 + \frac{1}{2}\varepsilon_q^2 + \frac{1}{2}\varepsilon_d^2 \tag{24}$$

Also, to guarantee the stability of the overall system, it is necessary that [31]:

$$\frac{dY_{MSC}}{dt} \prec 0 \tag{25}$$

So, the general asymptotic stability is assured. The NBA rules for MSC are chosen as:

$$v_{q-ref} = \omega_e\psi_f + R_g i_q + L_s\omega_e i_d + L_s\frac{di_{q-r}}{dt} + L_s\, k_q\varepsilon_q \tag{26}$$

$$v_{d-ref} = L_s k_d\varepsilon_d - L_s\omega_e i_q + R_g i_d \tag{27}$$

Figure 3 depicts a control diagram for the MSC using the NBA.

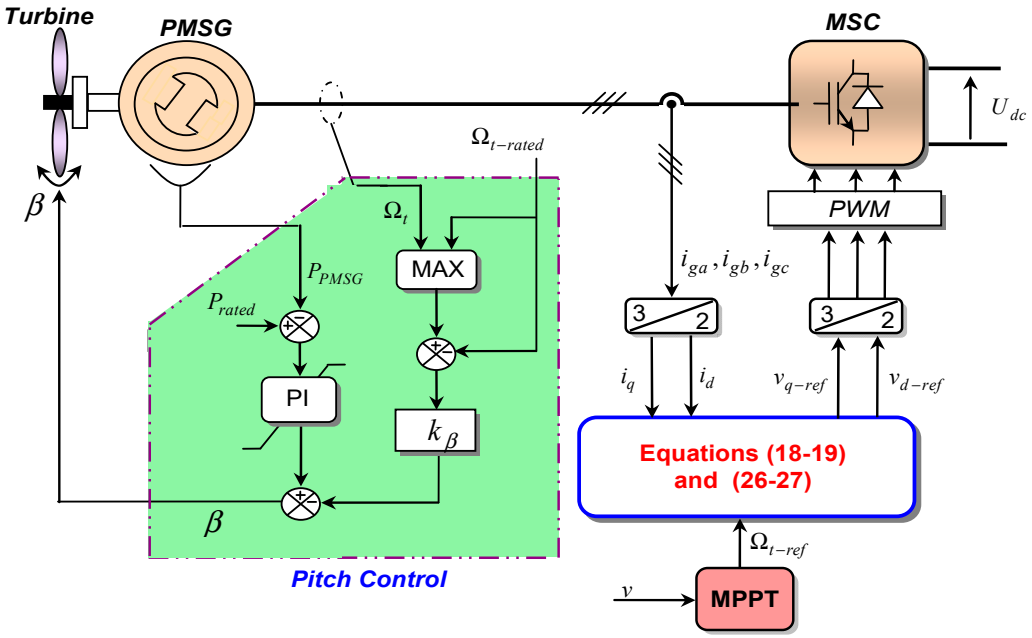

Figure 3. Control diagram for MSC with the NBA.

3.2. Control of GSC

Based on Equations (13) and (14), we can deduce that the powers can be controlled with i_{d-f} and i_{q-f}. Also, i_{d-f-r} is obtained by control of the DC bus voltage. As a result, controlling GSC involves two main tasks: first, an external voltage loop is utilized for keeping the DC bus voltage constant, and second, two inner current loops are employed to regulate the grid current and to perform power factor correction. Through Equations (12) and (13), we can write:

$$C\frac{dU_{dc}}{dt} = i_0 - \frac{3}{2}\frac{V}{U_{dc}}i_{d-f} \tag{28}$$

Thus, the following can be obtained:

$$U_{dc}C\frac{dU_{dc}}{dt} = \frac{C}{2}\frac{dU_{dc}^2}{dt} = P_{Turbine} - P_{grid} \tag{29}$$

Accordingly, the bus voltage regulator is responsible for providing the active power reference. Also, Equation (29) can be written as:

$$\frac{dU_{dc}^2}{dt} = \frac{2}{C}(P_{Turbine} - \frac{3}{2}Vi_{d-f}) \tag{30}$$

Then, we define the following errors:

$$\varepsilon_{DC} = U_{dc-ref}^2 - U_{dc}^2 \tag{31}$$

On the other hand:

$$\frac{d\varepsilon_{DC}}{dt} = \frac{dU_{dc-ref}^2}{dt} - \frac{2}{C}(P_{Turbine} - \frac{3}{2}V_0 i_{d-f-r}) \tag{32}$$

The major objective is to control U_{dc}. Consequently, i_{d-f} is utilized as a virtual adjustment variable to adapt ε_{DC}. Finally, U_{dc} converges toward U_{dc-ref} if we choose the following equation:

$$i_{d-f-r} = \frac{1}{V}\left[\frac{2}{3}P_{Turbine} - \frac{C}{3}(\frac{dU_{dc-ref}^2}{dt} + k_{DC}\varepsilon_{DC})\right] \tag{33}$$

where k_{DC} is the feedback invariable of the closed loop. On the other hand, to achieve the second purpose of GSC, the errors are defined using i_{q-f} and i_{d-f}:

$$\varepsilon_{d-f} = i_{d-f-r} - i_{d-f} \tag{34}$$

$$\varepsilon_{q-f} = i_{q-f-r} - i_{q-f} \tag{35}$$

The time derivatives of these errors are given as:

$$\frac{d\varepsilon_{d-f}}{dt} = \frac{di_{d-f-r}}{dt} - \frac{di_{d-f}}{dt} = \frac{di_{d-f-r}}{dt} - \frac{1}{L_f}(e_d - V - R_f i_{d-f} + L_f \omega i_{q-f}) \tag{36}$$

$$\frac{d\varepsilon_{q-f}}{dt} = \frac{di_{q-f-r}}{dt} - \frac{di_{q-f}}{dt} = \frac{di_{q-f-r}}{dt} - \frac{1}{L_f}(e_q - L_f \omega i_{d-f} - R_f i_{q-f}) \tag{37}$$

Considering the Lyapunov function, to found the stabilizing condition, as:

$$Y_{GSC} = \frac{1}{2}\varepsilon_{DC}^2 + \frac{1}{2}\varepsilon_{d-f}^2 + \frac{1}{2}\varepsilon_{q-f}^2 \tag{38}$$

Then, we can prove that to guarantee that $\frac{dY_{GSC}}{dt} \prec 0$ and the general asymptotic stability is assured if the NBA rules, for GSC, are chosen as:

$$v_{d-f-r} = \frac{3L_f}{C} V \varepsilon_{DC} + L_f \frac{di_{d-f-r}}{dt} + V + R_f i_{d-f} + L_f k_{d-f} \varepsilon_{d-f} - L_f \omega i_{q-f} \tag{39}$$

$$v_{q-f-r} = R_f i_{q-f} + L_f k_{q-f} \varepsilon_{q-f} + L_f \omega i_{d-f} \tag{40}$$

Figure 4 depicts the control diagram for GSC using the NBA.

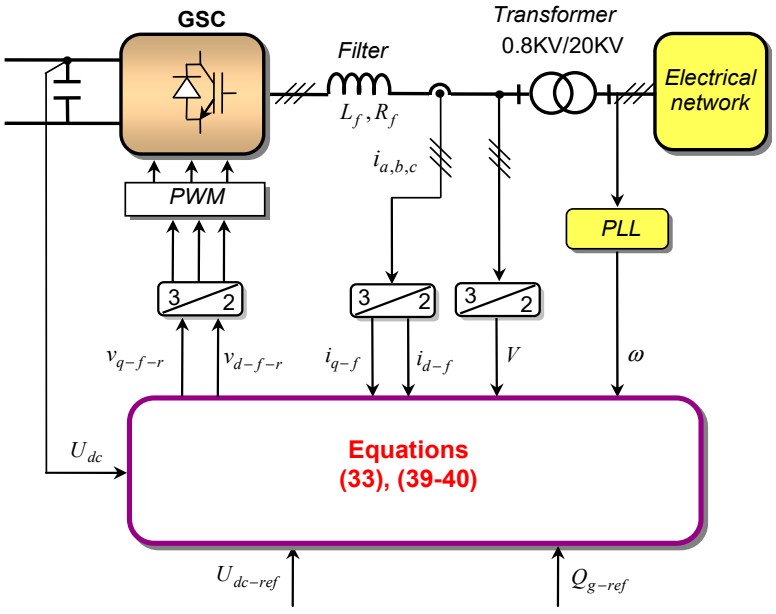

Figure 4. Nonlinear control of GSC.

3.3. Global Stability Analysis of the Presented Strategy

From (24), the time derivative of Y_{MSC} is:

$$\frac{dY_{MSC}}{dt} = \varepsilon_\Omega \frac{d\varepsilon_\Omega}{dt} + \varepsilon_d \frac{d\varepsilon_d}{dt} + \varepsilon_q \frac{d\varepsilon_q}{dt} \tag{41}$$

Using Equations (15)–(17) and (20)–(23), the following can be obtained:

$$\begin{aligned}\varepsilon_\Omega \tfrac{d\varepsilon_\Omega}{dt} &= \varepsilon_\Omega \tfrac{d\Omega_{t-ref}}{dt} - \tfrac{\varepsilon_\Omega}{J}\left[\tfrac{3}{2}p_n\left(\psi_f i_q\right) - T_m - F_v\Omega_t\right] \\ &= -k_\Omega\varepsilon_\Omega^2 + \tfrac{\delta_\Omega}{J}(Jk_\Omega\varepsilon_\Omega + T_m - \tfrac{3}{2}p_n\psi_f i_q + F_v\Omega_t + J\tfrac{d\Omega_{t-ref}}{dt})\end{aligned} \tag{42}$$

$$\begin{aligned}\varepsilon_d \tfrac{d\varepsilon_d}{dt} &= \varepsilon_d\left[-\tfrac{1}{L_s}(v_{md} + L_s\omega_e i_q - R_g i_d)\right] \\ &= -k_d\varepsilon_d^2 + \tfrac{\varepsilon_d}{L_s}\left[-v_{md} - L_s\omega_e i_q + R_g i_d + L_s k_d\varepsilon_d\right]\end{aligned} \tag{43}$$

$$\begin{aligned}\varepsilon_q \tfrac{d\varepsilon_q}{dt} &= \varepsilon_q\left[\tfrac{di_{q-r}}{dt} - \tfrac{di_q}{dt}\right] \\ &= -k_q\varepsilon_q^2 + \tfrac{\varepsilon_q}{L_s}\left[L_s\tfrac{di_{q-r}}{dt} - v_{mq} + \omega_e\psi_f + R_g i_q + L_s\omega_e i_d + k_q L_s\varepsilon_q\right]\end{aligned} \tag{44}$$

Using Equations (42)–(44), we can rewrite (41) as:

$$\begin{aligned}&\tfrac{dY_{MSC}}{dt} = -k_\Omega\varepsilon_\Omega^2 + \tfrac{\varepsilon_\omega}{J}(T_m - \tfrac{3}{2}p_n\psi_f i_q + F_v\Omega_t + Jk_\Omega\varepsilon_\Omega + J\tfrac{d\Omega_{t-ref}}{dt}) \\ &-k_d\varepsilon_d^2 + \tfrac{\varepsilon_d}{L_s}\left[-v_{gd} - L_s\omega_e i_q + R_g i_d + L_s k_d\varepsilon_d\right] \\ &-k_q\varepsilon_q^2 + \tfrac{\varepsilon_q}{L_s}\left[L_s\tfrac{di_{q-r}}{dt} - v_{mq} + \omega_e\psi_f + R_g i_q + L_s\omega_e i_d + k_q L_s\varepsilon_q\right]\end{aligned} \tag{45}$$

Substituting control laws (18), (19), (26) and (27) into (45), we obtain the following:

$$\frac{dY_{MSC}}{dt} = -k_\Omega\varepsilon_\omega^2 - k_d\varepsilon_d^2 - k_q\varepsilon_q^2 \le 0 \tag{46}$$

Based on the above analysis, it can be concluded that the stability of the MSC is ensured and major control objective is assured. On the other hand, based on (38), the time derivative of Y_{GSC} is:

$$\frac{dY_{GSC}}{dt} = \varepsilon_{DC}\frac{d\varepsilon_{DC}}{dt} + \varepsilon_{q-f}\frac{d\varepsilon_{q-f}}{dt} + \varepsilon_{d-f}\frac{d\varepsilon_{d-f}}{dt} \tag{47}$$

Using Equations (31), (32) and (34)–(37), the following can be obtained:

$$\begin{aligned}\varepsilon_{DC}\tfrac{d\varepsilon_{DC}}{dt} &= \varepsilon_{DC}\left[\tfrac{dU_{dc-ref}^2}{dt} - \tfrac{2}{C}(P_{Turbine} - \tfrac{3}{2}Vi_{d-f-r})\right] \\ &= -k_{DC}\varepsilon_{bus}^2 + \varepsilon_{DC}\left[\tfrac{dU_{dc-ref}^2}{dt} - \tfrac{2}{C}(P_{Turbine} - \tfrac{3}{2}Vi_{d-f-ref}) + k_{DC}\varepsilon_{DC}\right]\end{aligned} \tag{48}$$

$$\begin{aligned}\varepsilon_{d-f}\tfrac{d\varepsilon_{d-f}}{dt} &= \varepsilon_{d-f}\left[\tfrac{di_{d-f-r}}{dt} - \tfrac{1}{L_f}(e_d + L_f\omega i_{q-f} - V - R_f i_{d-f})\right] \\ &= -k_{d-f}\varepsilon_{d-f}^2 + \tfrac{\varepsilon_{d-f}}{L_f}\left[k_{d-f}L_f\varepsilon_{d-f} + L_f\tfrac{di_{d-f-r}}{dt} - L_f\omega i_{q-f} - e_d + V + R_f i_{d-f}\right]\end{aligned} \tag{49}$$

$$\begin{aligned}\varepsilon_{q-f}\tfrac{d\varepsilon_{q-f}}{dt} &= \varepsilon_{q-f}\left[-\tfrac{di_{q-f}}{dt}\right] \\ &= -k_{q-f}\varepsilon_{q-f}^2 + \tfrac{\varepsilon_{q-f}}{L_f}\left[-e_q + R_f i_{q-f} + L_f\omega\, i_{d-f} + k_{q-f}L_f\varepsilon_{q-f}\right]\end{aligned} \tag{50}$$

Using Equations (48)–(50), (47) can be rewritten as:

$$\begin{aligned}\tfrac{dY_{GSC}}{dt} = \;& -k_{q-f}\varepsilon_{q-f}^2 - k_{DC}\varepsilon_{DC}^2 - k_{d-f}\varepsilon_{d-f}^2 \\ &+ \tfrac{\varepsilon_{d-f}}{L_f}\left[\tfrac{3L_f}{C}V\varepsilon_{DC} + L_f\tfrac{di_{d-f-r}}{dt} - \varepsilon_d + k_{d-f}L_f\varepsilon_{d-f} + R_f i_{d-f} - L_f\omega i_{q-f} + V\right] \\ &+ \tfrac{\varepsilon_{q-f}}{L_f}\left[-\varepsilon_q + R_f i_{q-f} + L_f\omega i_{d-f} + k_{q-f}L_f\varepsilon_{q-f}\right]\end{aligned} \tag{51}$$

Substituting control laws (33), (39) and (40) into (51), we obtain the following:

$$\frac{dY_{GSC}}{dt} = -k_{DC}\varepsilon_{DC}^2 - k_{q-f}\varepsilon_{q-f}^2 - k_{d-f}\varepsilon_{d-f}^2 \le 0 \tag{52}$$

Based on the above analysis, it can be inferred that the stability of GSC is ensured.

3.4. Pitch Control Approach

The implanted WEGS has two functioning regions conforming to the speed of wind. Indeed, if the wind speed is inferior to the nominal wind speed, v_n, the speed of the WT is controlled at the optimal value so that the MPPT is ensured. So, β is set at zero and C_p is maximized. In contrast, under high-wind conditions, the MPPT approach is disabled and the adopted technique must diminish the massive amount of the mechanical power and limit the aerodynamic power captured by the WT by employing Pitch Control Technique (PCT) [32,33]. So, where the speed of wind surpasses v_n, the pitch angle approach is activated to limit the velocity of the WT and the extracted power at their rating by increasing the pitch angle, β. Also, the WT performs at lower effectiveness, less than $C_{p-\max}$. Figure 3 illustrates the employed PA configuration.

4. Performance Evaluation

To verify the presented strategy, a WEGS-based PMSG was simulated with Simulink. The characteristics of the WEGS are listed in Tables 1 and 2. Also, we fixed $Q_{g-ref} = 0\ VAR$ and $U_{dc-ref} = 1400\ V$. The configuration and control approach used are depicted in Figures 1, 3 and 4. The PLL system was employed to track the fundamental frequency and phase of grid voltage. On other hand, three cases were considered. The first case dealt with the testing of the presented methods under varying wind conditions. In the second case, the WEGS was tested under mechanical and electrical parameter variations. In the last step, the third scenario depicted the behavior of the WEGS during grid voltage sag conditions. Furthermore, the system performances under the proposed NBA were compared with those of the conventional VC method.

Table 1. Parameters of the PMSG.

Parameter	Value
P_r, rated power	2 (MW)
ω_m, rated mechanical speed	2.57 (rd/s)
R, stator resistance	0.008 (Ω)
L_s, stator d-axis inductance	0.0003 (H)
ψ_f, flux density	3.86 (wb)
p_n, pole pairs	60

Table 2. Parameters of the turbine.

Parameter	Value
ρ, air density	1.08 kg/m^3
A, area swept by blades	4775.94 m^2
v_n, base wind speed	12.4 m/s

4.1. Scenario 1: Performances of the Presented Methods Using Varying Wind Speed

Figure 5a shows the time-varying speed of wind. Figure 5c shows the coefficient of power, which is reserved at the maximum value $C_{p-\max}$ despite all the variations in the wind speed and whether the wind speed was inferior to the rated wind speed, $v_n = 12.4$ m/s. Similarly, Figure 5d depicts λ, which is close to its optimal value, $\lambda_{opti} = 8.1$. The proposed approach controls the velocity of the WT following variations in wind speed to maintain the λ_{opti}. But, it they are reduced in the elevated wind speed region conforming to the augment of β as shown in Figure 5b,d. The proposed technique regulates blade angle values conforming to the speed of wind. So, this pitch angle strategy limits the WT power and the PMSG velocity to their rated values as depicted in Figure 5e,f. Figure 5f illustrates the optimal speed, Ω_{t-ref}, versus the actual speed of the WT. As shown in Figure 5f, the speed of the WT follows the reference without any overshoot and attains a stable state. Figure 6 depicts the grid's current and voltage. It is obvious that the NBA scheme

guarantees perfect sine voltage injection to the electrical network. Figure 7 illustrates the DC bus voltage, which is well sustained at the reference value during diverse wind speed.

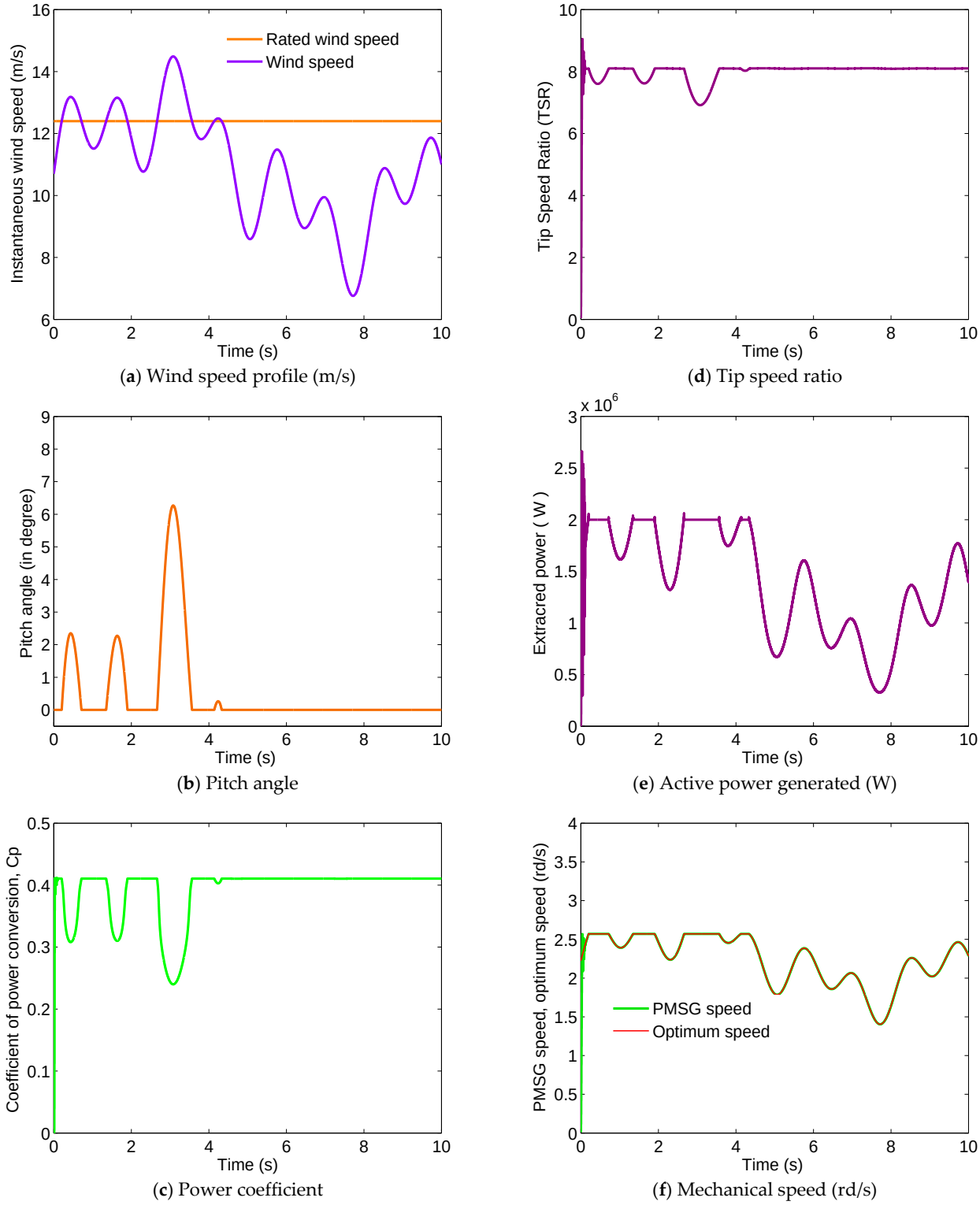

(**a**) Wind speed profile (m/s)

(**d**) Tip speed ratio

(**b**) Pitch angle

(**e**) Active power generated (W)

(**c**) Power coefficient

(**f**) Mechanical speed (rd/s)

Figure 5. WEGS characteristics using the proposed NBA.

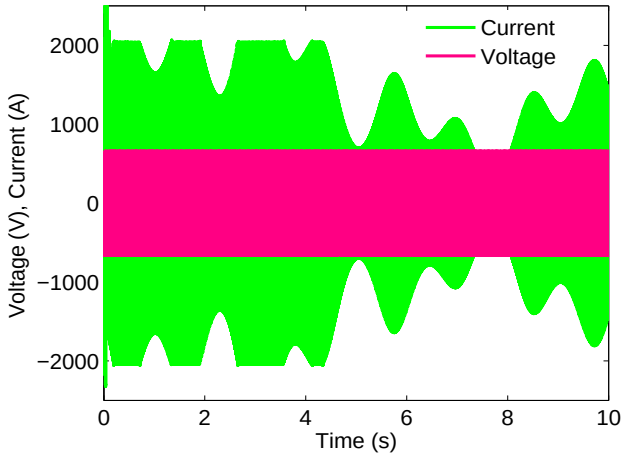

(**a**) Voltage and current of the grid.

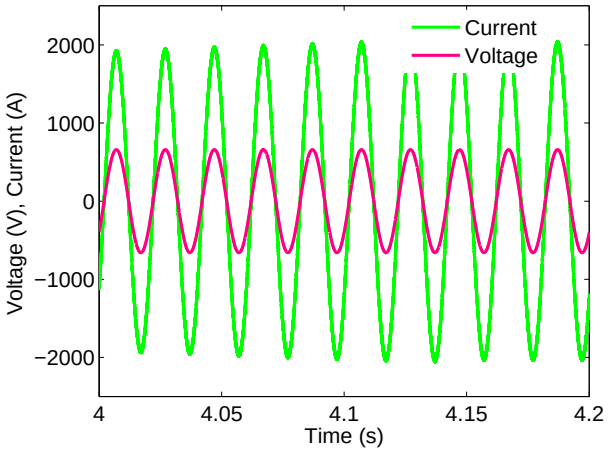

(**b**) The enlarged view related to voltage and current

Figure 6. Voltage and current of the grid.

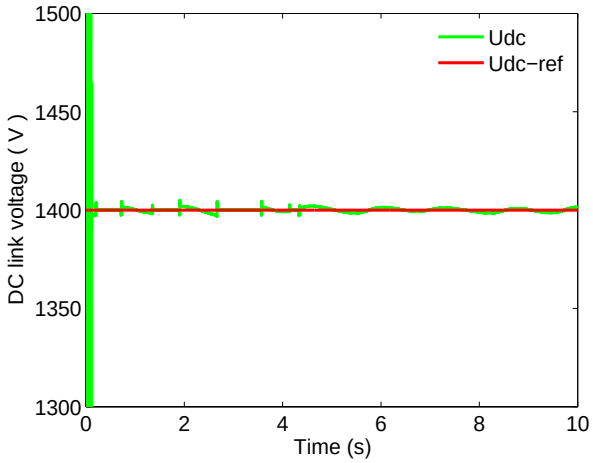

Figure 7. DC bus voltage (V).

4.2. Scenario 2: Impact of Parameter Variations

In the previous paragraph, we assumed that the system parameters are fixed. In this section, parameter uncertainty is introduced in the WEGS model to further investigate the performance of the presented approach to examine robustness of the studied method under the effects of parameter variations. Increases in these parameters are used in a scale of proportionality to the respective nominal values. So, a 50% increase in the values of stator resistance, stator inductance and total moment of inertia was taken into account. In addition, in Figures 8 and 9, 'A' refers to curves related to nominal parameters and 'B' refers to curves related to parameters with variations. It is quite clear that the parameter variations performed on the WEGS model generated apparent effects on the curves of PMSG speed and coefficient of power (Figures 8 and 9). Indeed, the NBA ensures a quicker response, inferior overshoot and fluctuations and has shorter settling time. This is because of the design of the VC, which depends on linearization around operating points. Therefore, the performances of the VC degrade if the system operation is far from its functioning points. As a result, the NBA performances are slightly more affected under the variations of parameter than under the VC approach.

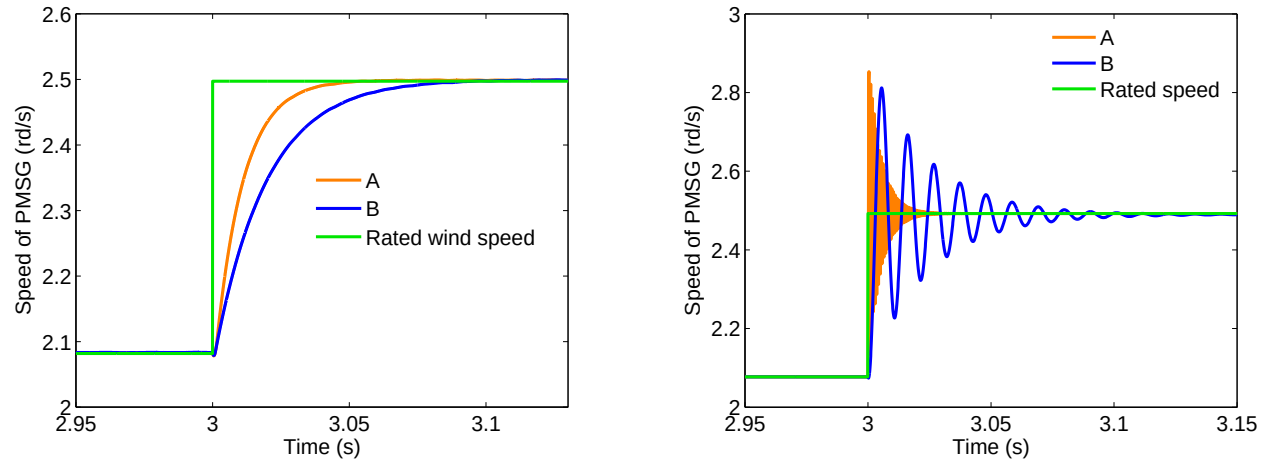

(**a**) NBA (**b**) VC approach

Figure 8. Speed of the PMSG (rd/s).

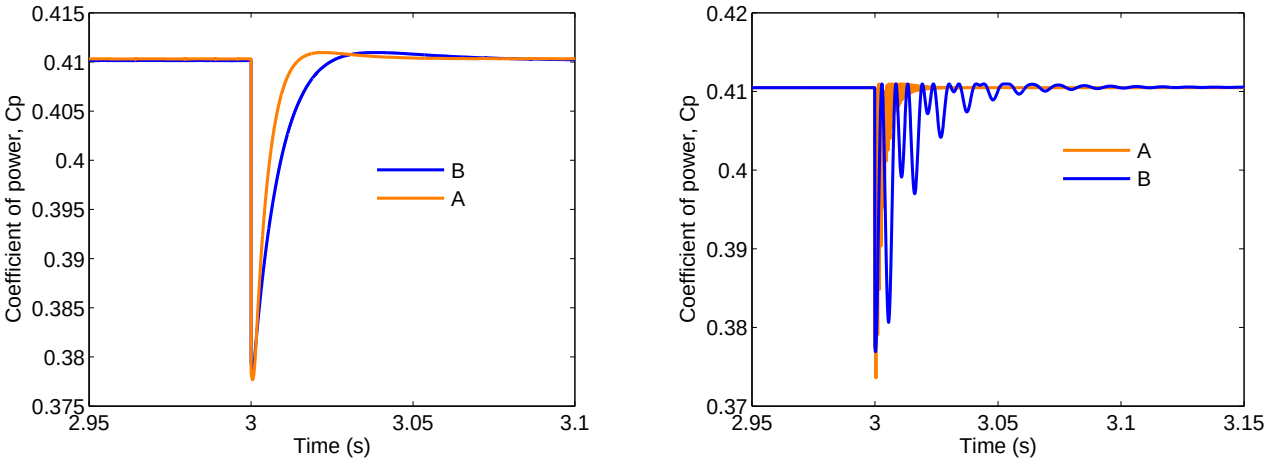

(**a**) NBA (**b**) VC approach

Figure 9. Power coefficient.

4.3. Scenario 3: Performance of the Proposed Methods under Grid Voltage Sag Conditions

To authenticate the qualities of the presented methods, this part presents the behavior of the WEGS during a network disturbance owing to a fault that may happen and which can lead to a voltage drop. The response of the NBA scheme for transient circumstances has been compared with that of the VC technique. The event occurred at time t = 3,8 s (Figure 1) in Bus 1. The fault was cleared at t = 4 s. Figures 10 and 11 depict the three-phase voltage during the appearance of a voltage drop in the electrical network. The results confirm that the voltage response using the NBT approach was dampened better compared to that realized when using VC method. Indeed, Figures 10 and 11 show that the proposed NBA method completed a much quicker reaction and lesser peak overshoot than the VC approach. Also, the NBA caused a lower ripple under the grid's fault. However, the transient performance of the three-phase voltage of the proposed NBA scheme during the disturbance was smoother and had fewer fluctuations than that of the VC approach. From Figure 12, in the method studied, the frequency waveform has fewer fluctuations compared to the VC approach during transients. In addition, the method studied ensures a smoother steady-state response and quicker transient response with fewer fluctuations under fault.

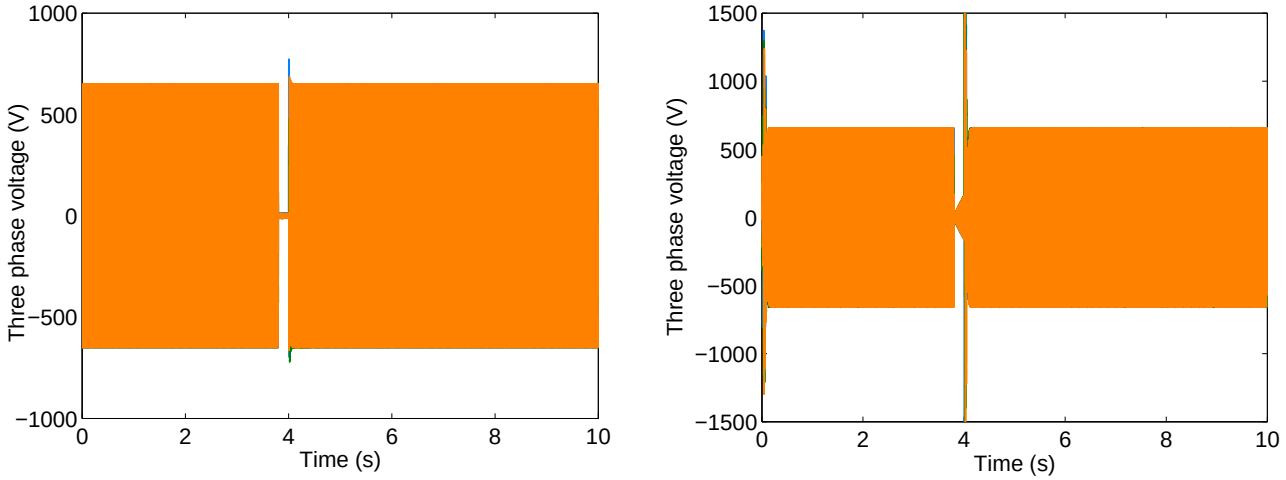

(**a**) NBA (**b**) VC approach

Figure 10. Voltage at Bus 1.

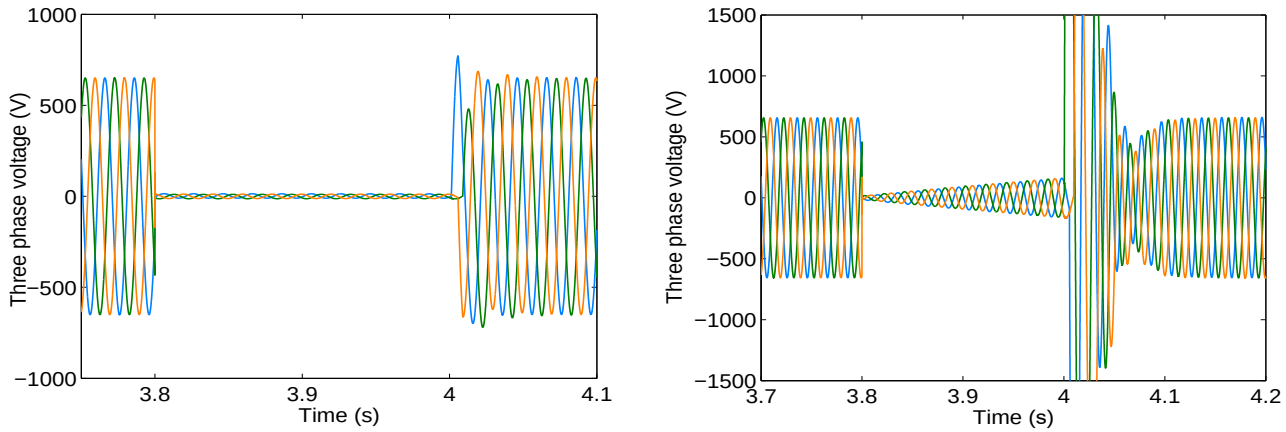

(**a**) NBA (**b**) VC approach

Figure 11. Zoom-in view of voltage at Bus 1.

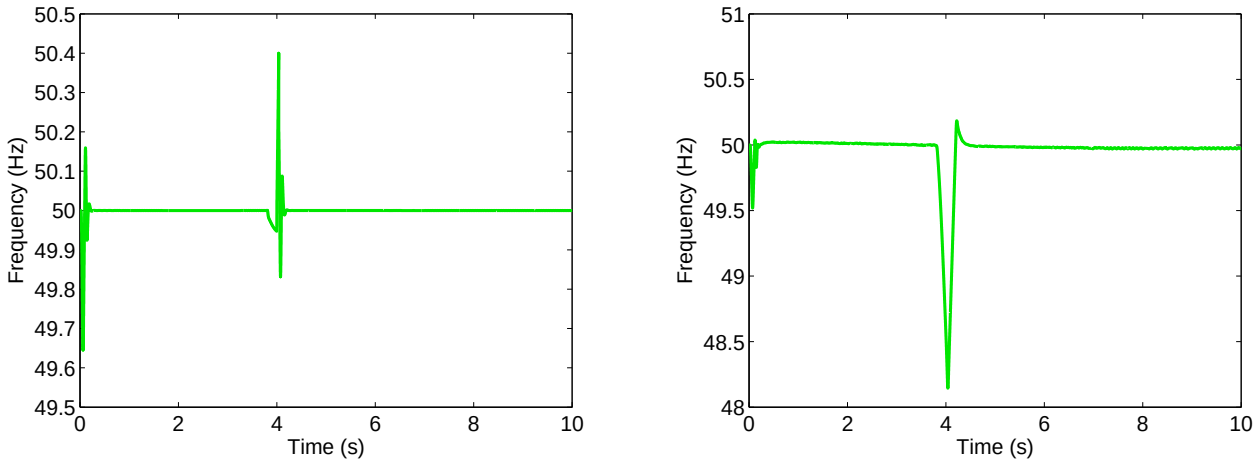

(**a**) NBA (**b**) VC approach

Figure 12. Frequency response of the system under grid voltage sag conditions.

5. Conclusions

This study proposes a Nonlinear Backstepping Approach (NBA) for a WEGS-based PMSG. The proposed approach is chosen to extract the maximum power, to regulate DC link voltage, to control powers exchanged and to guarantee the UPF under diverse functioning conditions. Numerical simulations are presented for different grid voltage conditions and under parameter deviations. Using the Lyapunov stability theory, some adequate conditions have been derived that guarantee the global asymptotical stability of the system. Compared with the VC approach, the simulation illustrated the superior performance of the proposed NBA method in terms of response time and overshoot. Also, it can be observed that maximum frequency deviations are reduced from 1.85 Hz to less than 0.4 Hz with the NBA. On the other hand, a test was also included in this work to verify the robustness of the NBA against variations in parameters. The NBA presents a very high immunity against low voltage drop conditions caused by symmetrical Three-Line-to-Ground faults (3LG). According to our investigation, the limitation of these presented approaches is the use of wind speed sensors. So, building on the findings and developed strategies, future works will be focused on the estimation of aerodynamic torque and the calculation of a reference value for the WT speed.

Author Contributions: Conceptualization, Y.E.; Methodology, A.O.; Validation, Y.E. and A.O.; Formal analysis, Y.E., S.S. and M.A.; Investigation, Y.E.; Resources, A.O.; Writing – original draft, S.S. and M.A. All authors have read and agreed to the published version of the manuscript.

Funding: This research received no external funding.

Institutional Review Board Statement: Not applicable.

Informed Consent Statement: Not applicable.

Data Availability Statement: The original contributions presented in the study are included in the article, further inquiries can be directed to the corresponding author.

Conflicts of Interest: The authors declare no conflict of interest.

Nomenclature

Symbol	Designation
$P_{Turbine}$	Aerodynamic power of the wind turbine
ρ	Air density
C_P	Coefficient of power conversion
v_w	Speed of the wind
λ	Ratio between the speed of the blade
R_t	Radius of the WT blade
ω_m	Rotor angular speed
ω_e	Electrical rotating velocity of the PMSG
T_m	Turbine's torque
Ω_t	Speed of the blades
β	Pitch Angle (PA) of the blade
Ω_{t-ref}	Reference of speed
v_{gd}, v_{gq}	Stator voltages
i_d, i_q	d-q axis stator currents
R_g	Stator resistance
L_s	Stator reactance of the PMSG
ψ_f	Peak flux of the PMSG
p_n	Number of pole pairs
T_e	Electromagnetic torque
J	Total moment of inertia of the system
F	Coefficient of viscous friction
v_{abc}	Grid voltage component voltages
i_{abc}	Line currents

L_f,R_f	Filter inductance and filter resistance
v_d,v_q	Grid voltage components in the d-axis and q-axis voltage components
V	Grid voltage components in the d-axis
e_d, e_q	GSC voltage components
U_{dc}	Voltage of DC link
ω	Electrical frequency
i_{dc}	Current at the input of the inverter
i_0	Output current of the PMSG
i_{d-grid}, i_{q-grid}	d-axis current and q-axis current of grid
C	Capacitor of DC link
Abbreviations	
WEGS	Wind Energy Generation System
PMSG	Permanent Magnet Synchronous Generator
MPPT	Maximum Power Point Tracking
NBA	Nonlinear Backstepping Approach
VC	Vector Controller
IG	Induction Generator
DFIG	Doubly Fed Induction Generator
BTBC	Back-to-Back Converter
UPF	Unity Power Factor
VCA	Vector Control Approach
LC	Linear Controller
PI	Proportional Integral
SMC	Sliding Mode Control

References

1. Shutari, H.; Ibrahim, T.; Nor, N.B.M.; Saad, N.; Tajuddin, M.F.N.; Abdulrab, H.Q. Development of a Novel Efficient Maximum Power Extraction Technique for Grid-Tied VSWT System. *IEEE Access* **2022**, *10*, 101922–101935. [CrossRef]
2. Salem, A.A.; Aldin, N.A.N.; Azmy, A.M.; Abdellatif, W.S. Implementation and Validation of an Adaptive Fuzzy Logic Controller for MPPT of PMSG-Based Wind Turbines. *IEEE Access* **2021**, *9*, 165690–165707. [CrossRef]
3. Mayilsamy, G.; Natesan, B.; Joo, Y.H.; Lee, S.R. Fast Terminal Synergetic Control of PMVG-Based Wind Energy Conversion System for Enhancing the Power Extraction Efficiency. *Energies* **2022**, *15*, 2774. [CrossRef]
4. Osman, A.; Alsokhiry, F. Sliding Mode Control for Grid Integration of Wind Power System Based on Direct Drive PMSG. *IEEE Access* **2022**, *10*, 26567–26579. [CrossRef]
5. Bakbak, A.; Altintas, M.; Ayaz, M.; Canseven, H.T.; Boztepe, M.; Akin, O.; Mese, E. PMSG-Based Dual-Port Wind-Energy Conversion System With Reduced Converter Size. *IEEE Access* **2021**, *9*, 118953–118967. [CrossRef]
6. Kim, C.; Kim, W. Low-Voltage Ride-Through Coordinated Control for PMSG Wind Turbines Using De-Loaded Operation. *IEEE Access* **2021**, *9*, 66599–66606. [CrossRef]
7. Shariatpanah, H.; Fadaeinedjad, R.; Rashidinejad, M. A New Model for PMSG-Based Wind Turbine with Yaw Control. *IEEE Trans. Energy Convers.* **2013**, *28*, 929–937. [CrossRef]
8. Li, S.; Haskew, T.A.; Swatloski, R.P.; Gathings, W. Optimal and Direct-Current Vector Control of Direct-Driven PMSG Wind Turbines. *IEEE Trans. Power Electron.* **2012**, *27*, 2325–2337. [CrossRef]
9. Trinh, D.T.; Wu, Y.K.; Pham, M.H. Adaptive Frequency Control Strategy for PMSG-Based Wind Turbines with Improved Rotor Speed Recovery. *IEEE Access* **2024**, *12*, 63853–63864. [CrossRef]
10. Rajaei, A.; Mohamadian, M.; Yazdian Varjani, A. Vienna-Rectifier-Based Direct Torque Control of PMSG for Wind Energy Application. *IEEE Trans. Ind. Electron.* **2013**, *60*, 2919–2929. [CrossRef]
11. Tian, Y.; Cai, B.; Liu, Y. Research on BPNN-Based SVM-DTC for Direct Drive PMSG Wind Turbine. In Proceedings of the 2021 China Automation Congress (CAC), Beijing, China, 22–24 October 2021; pp. 3098–3103. [CrossRef]
12. Zhang, Z.; Wang, F.; Wang, J.; Rodríguez, J.; Kennel, R. Nonlinear Direct Control for Three-Level NPC Back-to-Back Converter PMSG Wind Turbine Systems: Experimental Assessment with FPGA. *IEEE Trans. Ind. Inform.* **2017**, *13*, 1172–1183. [CrossRef]
13. Zhang, Z.; Zhao, Y.; Qiao, W.; Qu, L. A Space-Vector Modulated Sensorless Direct-Torque Control for Direct-Drive PMSG Wind Turbines. *IEEE Trans. Ind. Appl.* **2014**, *50*, 2331–2341. [CrossRef]
14. Zhang, Z.; Zhao, Y.; Qiao, W.; Qu, L. A Discrete-Time Direct-Torque Control for Direct-Drive PMSG-Based Wind Energy Conversion Systems. *IEEE Trans. Ind. Appl.* **2015**, *51*, 3504–3514. [CrossRef]
15. Freire, N.M.A.; Cardoso, A.J.M. A Fault-Tolerant Direct Controlled PMSG Drive for Wind Energy Conversion Systems. *IEEE Trans. Ind. Electron.* **2014**, *61*, 821–834. [CrossRef]
16. Bakhtiari, F.; Nazarzadeh, J. Optimal Estimation and Tracking Control for Variable-speed Wind Turbine with PMSG. *J. Mod. Power Syst. Clean Energy* **2020**, *8*, 159–167. [CrossRef]

17. Belkhier, Y.; Achour, A.; Ullah, N.; Shaw, R.N.; Farooq, Z.; Ullah, A.; Alzaed, A.N. Intelligent Energy-Based Modified Super Twisting Algorithm and Factional Order PID Control for Performance Improvement of PMSG Dedicated to Tidal Power System. *IEEE Access* **2021**, *9*, 57414–57425. [CrossRef]
18. Pan, L.; Shao, C. Wind energy conversion systems analysis of PMSG on offshore wind turbine using improved SMC and extended state observer. *Renew Energy* **2020**, *161*, 149–161. [CrossRef]
19. Jingfeng, M.; Aihua, W.; Guoqing, W.; Xudong, Z. Maximum power point tracking in variable speed wind turbine system via optimal torque sliding mode control strategy. In Proceedings of the 34th Chinese Control Conference (CCC), Hangzhou, China, 28–30 July 2015; pp. 7967–7971.
20. Wang, G.; Wai, R.; Liao, Y. Design of backstepping power control for grid-side converter of voltage source converter-based high-voltage dc wind power generation system. *IET Renew. Power Gener.* **2013**, *7*, 118–133. [CrossRef]
21. Khan, N.; Rahman, S.F.; Hinchey, M.J.; Rahman, M.A. Adaptive Backstepping Based Maximum Power Point Tracking Control For a Variable Speed Marine Current Energy Conversion System. In Proceedings of the IEEE Canadian Conference of Electrical and Computer Engineering (CCECE), Regina, SK, Canada, 5–8 May 2013; pp. 1–5. [CrossRef]
22. Kim, K.H.; Jeung, Y.C.; Lee, D.C.; Kim, H.G. LVRT scheme of PMSG wind power systems based on feedback linearization. *IEEE Trans. Power Electron.* **2012**, *27*, 2376–2384. [CrossRef]
23. Nasiri, M.; Milimonfared, J.; Fathi, S.H. Robust control of PMSG based wind turbine under grid fault conditions. *Indian J. Sci. Technol.* **2015**, *8*, 1. [CrossRef]
24. Mozayan, S.M.; Saad, M.; Vahedi, H.; Fortin-Blanchette, H.; Soltani, M. Sliding mode control of PMSG wind turbine based on enhanced exponential reaching law. *IEEE Trans. Ind. Electron.* **2016**, *63*, 6148–6159. [CrossRef]
25. Zheng, X.M.; Feng, Y.; Han, F.L.; Yu, X.H. Integral-type terminal sliding-mode control for grid-side converter in wind energy conversion systems. *IEEE Trans. Ind. Electron.* **2019**, *66*, 3702–3711. [CrossRef]
26. Errouissi, R.; Al-Durra, A. A novel PI-type sliding surface for PMSG-based wind turbine with improved transient performance. *IEEE Trans. Energy Convers.* **2018**, *33*, 834–844. [CrossRef]
27. Errami, Y.; Hilal, M.; Benchagra, M.; Ouassaid, M.; Maaroufi, M. Nonlinear control of MPPT and grid connected for variable speed wind energy conversion system based on the PMSG. *J. Theor. Appl. Inf. Technol.* **2012**, *39*, 204–217.
28. Hilal, M.; Benchagra, M.; Errami, Y.; Maaroufi, M.; Ouassaid, M. Maximum power tracking of wind turbine based on doubly fed induction generator. *Int. Rev. Model. Simul.* **2011**, *4*, 2255–2263.
29. Hossain, M.D.I.; Abido, M.A. Positive-Negative Sequence Current Controller for LVRT Improvement of Wind Farms Integrated MMC-HVDC Network. *IEEE Access* **2020**, *8*, 193314–193339. [CrossRef]
30. Nguyen, H.T.; Al-Sumaiti, A.S.; Al Hosani, K.; El Moursi, M.S. Multifunctional Control of Wind-Turbine Based Nano-Grid Connected to Distorted Utility-Grid. *IEEE Trans. Power Syst.* **2022**, *37*, 576–589. [CrossRef]
31. Errami, Y.; Ouassaid, M.; Maaroufi, M. Variable structure control for permanent magnet synchronous generator based wind energy conversion system operating under different grid conditions. In Proceedings of the 2nd World Conference on Complex Systems, WCCS 2014, Agadir, Morocco, 10–12 November 2014; pp. 340–345. [CrossRef]
32. Evangelista, C.; Fernando, V.; Paul, P. Active and reactive power control for wind turbine based on a MIMO 2-sliding mode algorithm with variable gains. *IEEE Trans. Energy Convers.* **2013**, *28*, 682–689. [CrossRef]
33. Thapa, K.B.; Jayasawal, K. Pitch Control Scheme for Rapid Active Power Control of a PMSG-Based Wind Power Plant. *IEEE Trans. Ind. Appl.* **2020**, *56*, 6756–6766. [CrossRef]

Disclaimer/Publisher's Note: The statements, opinions and data contained in all publications are solely those of the individual author(s) and contributor(s) and not of MDPI and/or the editor(s). MDPI and/or the editor(s) disclaim responsibility for any injury to people or property resulting from any ideas, methods, instructions or products referred to in the content.